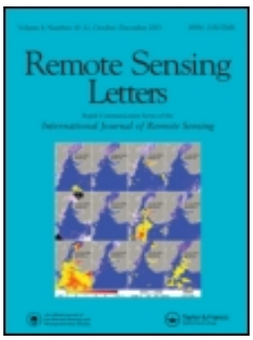

Remote Sensing Letters

ISSN: 2150-704X (Print) 2150-7058 (Online) Journal homepage: http://www.tandfonline.com/loi/trsl20

Road centreline extraction from classified images by using the geodesic method

Zelang Miao & Wenzhong Shi

To cite this article: Zelang Miao & Wenzhong Shi (2014) Road centreline extraction from classified images by using the geodesic method, Remote Sensing Letters, 5:4, 367-376, DOI: 10.1080/2150704X.2014.907935

To link to this article: http://dx.doi.org/10.1080/2150704X.2014.907935

Remote Sensing Letters, 2014
Vol. 5, No. 4, 367–376, http://dx.doi.org/10.1080/2150704X.2014.907935

Taylor & Francis
Taylor & Francis Group

Road centreline extraction from classified images by using the geodesic method

Zelang Miao[a,b] and Wenzhong Shi[a]*

[a]*Department of Land Surveying and Geo-Informatics, The Hong Kong Polytechnic University, Kowloon, Hong Kong;* [b]*School of Environmental Science and Spatial Informatics, China University of Mining and Technology, Xuzhou, Jiangsu, China*

(*Received 29 December 2013; accepted 19 March 2014*)

This study presents an automatic method for accurate road centreline extraction from classified images. Unlike earlier methods that have mainly relied on the thinning algorithm, the proposed automatic method selects end points from a classified image and then connects them using the geodesic method to formulate the road network. As the proposed method generates the road centreline by tracing along the ridge line of the optimally oriented flux (OOF) measure, this method is able to eliminate undesired spurs while retaining the correct road network topology. Three test images are used to quantitatively evaluate the proposed method. Experiments show that the proposed method yields a substantial improvement over the thinning algorithm.

1. Introduction

With the advent of modern acquisition sensors such as Satellite Pour l'Observation de la Terre (SPOT), IKONOS, and WorldView-2, very high resolution (VHR) satellite images have become increasingly available in recent years. Road extraction from these images is one of the most important applications of remote sensing, and this application has received much attention over the years, with various methods being proposed (Poullis and You 2010). According to the levels of information used, road extraction methods fall into three main categories: (1) *pixel-based*, (2) *region-based*, and (3) *knowledge-based* methods (Mena 2003; Das, Mirnalinee, and Varghese 2011). The most popular methods in recent years are *region-based*. These methods first segment images into objects and then follow a rule to refine road networks (Shi, Miao, and Debayle 2014). One set of studies has focused on road objects detection. These *region-based* methods use both the spectral information on roads (Treash and Amaratunga 2000) and their geometrical features (Miao et al. 2013; Shi et al. 2014). Incorporating both spectral and geometrical features can generally allow extraction of road segments with high accuracy.

Another set of studies has focused on road centreline extraction from the classified road segments produced by *region-based* methods. The thinning algorithm (Soille 1998) is one of the most commonly used region-based methods for centreline extraction. In general, the thinning algorithm involves iteratively identifying boundary points and removing those whose removal will not introduce/loss of topological and geometric features. This method has been shown to be efficient, but it always produces

*Corresponding author. Email: lswzshi@polyu.edu.hk

many spurious branches (i.e., spurs), which reduce smoothness and correctness of the centreline. To help resolve this limitation, the Radon transform (Zhang and Couloigner 2007) and the Hough transform (Poullis and You 2010) have been tried as means to extract centrelines from classified images. Locations of strong peaks in the transform matrix correspond to the location of straight lines in the original image. These two transform methods have shown good performance when dealing with straight road segments. However, such methods are not suitable for short and curvilinear lines. Therefore, a self-organized clustering method (Doucette et al. 2001) has been developed for road centreline extraction from classified images. This approach first identifies spatial cluster centres and then links these centres to derive road network topology. Despite its good performance, this approach, however, cannot extract centrelines located at the end of road segments.

Recently, a method from the field of computer vision known as the subspace constrained mean shift (SCMS) (Ozertem and Erdogmus 2011) has been investigated as a means to extract smooth centrelines from discrete noisy points. The SCMS method projects all input data points to the closest ridge of the probability density function (PDF), as generated by kernel density estimation (KDE). The results of the SCMS are smooth, robust, and have no spurs. However, the SCMS has to iteratively project all discrete points onto centrelines, which leads to a high computation load. Furthermore, the SCMS is a biased estimator (Genovese et al. 2013), which severely influences its accuracy. As indicated earlier, although automatic centreline extraction from classified images has received sustained attention, both robustness and accuracy remain elusive. Therefore, further studies are needed on the best means to extract accurate centrelines from classified images.

This study focuses on an automatic method for accurate road centreline extraction from classified images. The end points of a classified image (a pixel in a binary image is an end point if it has exactly one 8-connected neighbour) are extracted and then connected to create a central line that formulates the road network. The main contributions of this study are the following:

(1) proposing a method for end points detection from a classified image
(2) proposing an automatic method for accurate road centreline extraction from a classified image

2. Methodology

The aim of this study was to devise a computationally efficient approach to extract accurate centrelines from classified images. Figure 1 summarizes the proposed method.

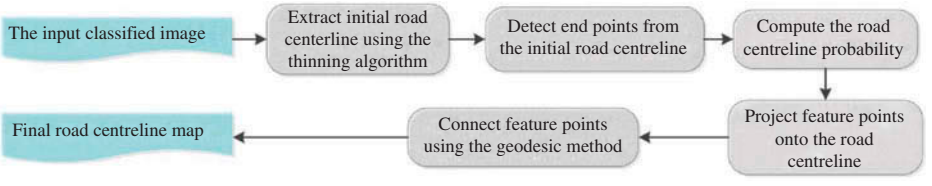

Figure 1. Flow chart of the proposed method.

The proposed method consists of three main steps, as follows:

Step 1: Extract the end points from the classified image.
Step 2: Compute the probability that each pixel is located on the road centreline using the optimally oriented flux (OOF) method and then project the end points onto ridge lines using the mean shift method.
Step 3: Link the projected end points by the geodesic method to create the central line and formulate the road network.

The details of each step are described in the following sections.

2.1. Detection of end points

The first step of the proposed method is to find the end points in the classified image. The classified image is partitioned into small regions using the k-means clustering algorithm. Suppose that the classified image C (road pixels in C are equal to 1 while non-road pixels 0) has M connected components (CCs). The k-means clustering algorithm is iteratively performed on each CC. For the ith connected component, CC_i, the number of clusters denoted as k_i is adaptively determined as

$$k_i = \begin{cases} 3 & , \text{if } A_i \leq 300 \text{ pixels} \\ \lceil A_i/100 \rceil, & \text{otherwise} \end{cases} \tag{1}$$

where $i = 1, \ldots, M$, $\lceil \cdot \rceil$ rounds a number up to the next integer, and A_i represents the area of CC_i. Any region with an area less than 300 pixels tends to be partitioned into one cluster using the k-means clustering algorithm. We enforce the k-means algorithm to segment regions with areas less than 300 pixels into 3 clusters. By doing so, we can detect the end points of small segments. After this partition of the classified image, the end regions are subsequently detected. The regions are dilated, and the label numbers of the dilated regions are judged. If a dilated region has only two label numbers, then that region is judged as the end region. The centroids of the end regions are taken as end points. An example of end point detection is depicted in Figure 2(*a*)–(*d*).

2.2. Computation of the road centreline probability

The road pixels identified in the classification process lead to an estimation of road centreline pixel probability. The possible road centre locations are taken as discrete joint random variables. Their probabilities of being located on the road centreline are computed by the OOF method (Law and Chung 2008, Benmansour and Cohen 2011). Let C be the classified image. The OOF measure at the point $\boldsymbol{x}$ is defined as

$$f(\boldsymbol{x}, \boldsymbol{v}; r) = \int_{\partial \mathrm{S}_r} ((\nabla (G * C)(\boldsymbol{x} + \boldsymbol{h}) \cdot \boldsymbol{v}) \boldsymbol{v}) \cdot \boldsymbol{n} \mathrm{d}a \tag{2}$$

where ∂ denotes a partial derivative, S_r is a local sphere centred at point $\boldsymbol{x}$ with the radius r, $*$ means the convolution operation, $\nabla(\cdot)$ is the gradient, G is a Gaussian function, $\boldsymbol{h}$ is the relative position vector along $\partial \mathrm{S}_r$, $\boldsymbol{n}$ is the outward unit normal of $\partial \mathrm{S}_r$, and $\mathrm{d}a$ is an infinitesimal area on $\partial \mathrm{S}_r$. The function f is the flux of the smoothed image gradient

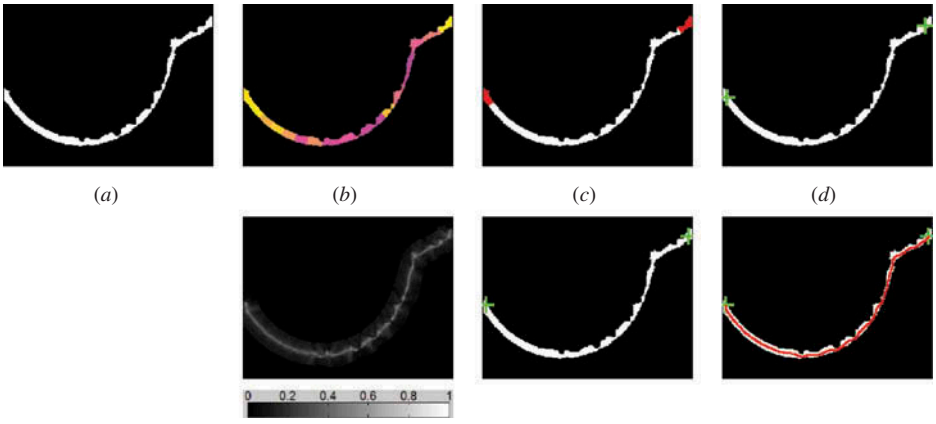

(*a*) (*b*) (*c*) (*d*) (*e*) (*f*) (*g*)

Figure 2. End points detection: (*a*) the classified image where 'white' and 'black' denote *road* and *non-road* pixels, respectively; (*b*) the partitioning result; (*c*) end regions detection result (end regions are shown in red); (*d*) end points, where $\boldsymbol{x}_0 = (94, 5), \boldsymbol{x}_1 = (22, 205)$, are shown in green crosses; (*e*) the OOF measure result in which high value indicates high road centreline probability; (*f*) the adjustment result of initial end points, where $\boldsymbol{x}_0 = (89, 4), \boldsymbol{x}_1 = (20, 208)$, is shown in green cross; and (*g*) the connection result that is shown in red.

$\nabla(G * C)$, which is projected along direction $\boldsymbol{v}$ towards the sphere $\partial \mathrm{S}_r$. To detect curvilinear structures with higher intensity values than the background, we are interested in finding the structure direction at $\boldsymbol{x}$ that minimizes $f(\boldsymbol{x}, \boldsymbol{v}; r)$, and we use the following formula

$$\min_{\boldsymbol{v}} f\ (\boldsymbol{x}, \boldsymbol{v}; r)$$

where $r = [3, 5, 7, 9, 11]$. Using the divergence theorem (Spiegel, Lipschutz, and Spellman 2009), it can be shown that $f(\boldsymbol{x}, \boldsymbol{v}; r)$ can be calculated using a convolution operation as follows:

$$f(\boldsymbol{x}, \boldsymbol{v}; r) = \boldsymbol{v}^{\mathrm{T}}\{C * (\partial \boldsymbol{G}) * \mathbb{I}_{\mathrm{S}_r}(\boldsymbol{x})\}\boldsymbol{v} := \boldsymbol{v}^{\mathrm{T}}\{C * \boldsymbol{F}_r(\boldsymbol{x})\}\boldsymbol{v} \tag{3}$$

where $(\partial \boldsymbol{G})$ denotes the Hessian matrix of the Gaussian function $\boldsymbol{G}$, $\mathbb{I}_{\mathrm{S}_r}(\boldsymbol{x})$ is the indicator function inside the sphere S_r, and $\boldsymbol{F}_r(\boldsymbol{x}) = (\partial \boldsymbol{G}) * \mathbb{I}_{\mathrm{S}_r}(\boldsymbol{x})$ is called the oriented flux filter.

Figure 2(*e*) shows an example of an OOF measure result. As can be seen from this figure, pixels that are located on the centreline have large OOF values, but non-centreline pixels have low OOF values.

2.3. *Adjustment of end points*

The end points extracted in Section 2.1 may not precisely locate on the road centreline. Consequently, the result of linking the end points is likely to be biased relative to the true centreline. To overcome this shortcoming, the end points need to be pre-processed to obtain precise end points that locate on the road centreline. Therefore, the gradient ascent

method (Snyman 2005) is used to iteratively adjust initial end points to the road centreline. The gradient ascent is expressed as

$$\boldsymbol{x}^{(m+1)} = \boldsymbol{x}^{(m)} + \delta\left(\nabla \mathrm{OOF}\left(\boldsymbol{x}^{(m)}\right)\right) \tag{4}$$

where $\boldsymbol{x}^{(m)}$ is the pixel location in mth iteration of the gradient descent, δ is the step size, and $\nabla \mathrm{OOF}(\cdot)$ is the gradient of the OOF result. The gradient ascent is iteratively performed until the algorithm satisfies the convergence condition. An example of adjusting end points onto the road centreline is illustrated in Figure 2(*f*).

2.4. Connection of end points

After the adjustment described in Section 2.3, the end points are linked by the geodesic method (Peyré et al. 2009) to create the central line and formulate the road network. Consider a smooth curve $\gamma(t) : [0, 1] \rightarrow \Omega$ on an image where t denotes the parameter of the curve, and Ω is the image domain, which is defined as $\Omega = [0, 1]^2$. The smooth curve $\gamma(t)$ is generally constrained as

$$\{\gamma(t) : [0, 1] \rightarrow \Omega \backslash \gamma(0) = \boldsymbol{x}_0 \; and \; \gamma(1) = \boldsymbol{x}_1\} \tag{5}$$

where $\boldsymbol{x}_0$ and $\boldsymbol{x}_1$ denote the starting and ending points, respectively. Let $L(\gamma)$ denote the weighted length of $\gamma(t)$, which is computed using the formula

$$L(\gamma) = \int_0^1 W(\gamma(t))||\gamma'(t)||\mathrm{d}t \tag{6}$$

where $W(\cdot)$ is a weight function, and $\gamma'(t) \in \mathbb{R}^2$ is the derivative of $\gamma(t)$. For road network formulation, a road can be approximately defined as a smooth curve that has a constant kernel density value of $c \in \mathbb{R}$. Based on this definition of the road model, a weight function $W(\boldsymbol{x})$ can be defined as

$$W(\boldsymbol{x}) = |I(\boldsymbol{x}) - c| + \varepsilon \tag{7}$$

where I is the OOF measure described in Section 2.3, and ε (i.e., $\varepsilon = 0.01$) is a small value that prevents $W(\boldsymbol{x})$ from vanishing. In this study, the constant value c is fixed to $I(\boldsymbol{x}_0)$. The goal is to extract a curve γ^* that has the minimal length between two fixed points $\boldsymbol{x}_0$ and $\boldsymbol{x}_1$:

$$\gamma^* = \min_{\gamma \in (\boldsymbol{x}_0, \boldsymbol{x}_1)} L(\gamma) \tag{8}$$

where γ^* is called the minimal path. The end points are aligned to each other to create the central line that formulates the final road network. Figure 2(*g*) shows an example of linking the end points by using the geodesic method.

The advantages of the proposed geodesic method for linking the end points from the OOF result are as follows:

(1) The end points are adjusted to the centreline, and hence their initial positions have less influence on the final result.
(2) According to the OOF result, the geodesic method traces the true centreline, which tends to be well centred.

3. Test cases

In this section, several experiments to test the proposed method are described. The proposed method is also compared with other methods studied in the literature, to show the method's advantages or disadvantages. This study used MATLAB® (R2010b version) as the coding environment on a PC that had an Intel Core 2 Quad processor with a 2.83-GHz clock speed.

3.1. Classification

In this experiment, a spectral–spatial classification method for road extraction (Shi, Miao, and Debayle 2014) was selected for classifying satellite images. The first two test images were obtained by QuickBird. Both of these images had a spatial size of 512 pixels × 512 pixels. The third test image was obtained by WorldView-2 and had a spatial size of 400 pixels × 400 pixels. All three images were classified into five classes of surface: *road, building, grass, shadow*, or *water*. Some 5% of the ground truth data for each class were selected as the training samples. Figure 3 depicts the classification results for the three satellite images. Figure 3(*a*) and (*b*) are test images showing the ground truth data sets (which are shown in red) and the classification results, respectively. The user's accuracy and producer's accuracy (Campbell and Wynne 2011) were used to evaluate the accuracies of classification results, which are given in Table 1.

(*a*) (*b*) (*c*)

Figure 3. The test image of (*a*) Case 1, (*b*) Case 2, and (*c*) Case 3. The ground truth data sets are shown in red.

Table 1. Classification accuracies of three test images.

Case	User's accuracy (%)	Producer's accuracy (%)
1	63.19	63.70
2	66.03	51.45
3	59.45	67.73

3.2. Comparison with the existing methods

The results from comparing the proposed method with the thinning algorithm and SCMS methods are reported in this section. Figure 3 shows the test images and corresponding ground truth data sets. Road centrelines extracted by different methods are presented in Figure 4.

The results of the three centreline extraction methods show that the proposed method and the SCMS provided smoother results than the thinning algorithm. The thinning algorithm method produced many undesired spurs and branches, which reduced the smoothness of the road centreline. Although the SCMS extracted a smooth result, the estimate was a biased version of the true centreline, as the SCMS is a biased estimator. Also, the SCMS could not handle the junctions well.

The three methods were compared in terms of both their computation complexity and their accuracy. Three measures, as proposed by Wiedemann et al. (1998), were used to quantitatively evaluate the road centreline extraction accuracy, as follows

$$E_1 = (\mathrm{TP})/((\mathrm{TP}) + (\mathrm{FN})) \tag{9}$$

$$E_2 = (\mathrm{TP})/((\mathrm{TP}) + (\mathrm{FP})) \tag{10}$$

$$E_3 = (\mathrm{TP})/((\mathrm{TP}) + (\mathrm{FP}) + (\mathrm{FN})) \tag{11}$$

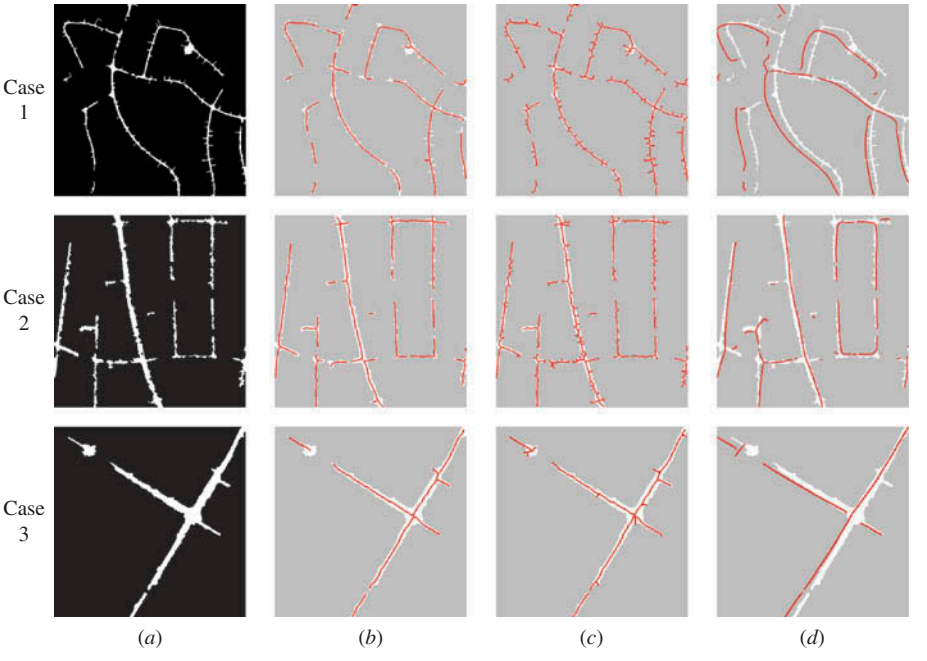

Figure 4. (*a*) Classification results where 'white' and 'black' denote *road* and *non-road* pixels, respectively; (*b*) results of the proposed method that are shown in red; (*c*) results of the thinning algorithm that are shown in red; and (*d*) SCMS results that are shown in red.

Table 2. Comparison of computation time for different centreline extraction methods.

Case	Number of points	Computation time (s)		
		The thinning algorithm	SCMS	The proposed method
1	12,565	1.01	101.27	51.45
2	18,334	1.58	162.19	46.59
3	9245	0.87	44.14	13.29

Table 3. Quantitative evaluation of different centreline extraction methods.

Method	Case 1			Case 2			Case 3		
	$E_1(\%)$	$E_2(\%)$	$E_3(\%)$	$E_1(\%)$	$E_2(\%)$	$E_3(\%)$	$E_1(\%)$	$E_2(\%)$	$E_3(\%)$
Thinning	85.09	76.10	67.15	64.40	79.09	55.03	70.58	81.17	60.65
SCMS	4.65	6.15	2.72	17.99	30.55	12.77	9.63	12.81	5.82
Proposed	80.65	88.35	72.89	60.61	91.01	57.16	67.63	88.47	62.15

where E_1, E_2, and E_3 are completeness, correctness, and quality, respectively. TP, FN, and FP represent, respectively, number of true positive (i.e., the lengths of matched extracted data within the buffer around the reference road data), number of false negative (i.e., the lengths of referenced data that did not locate within the buffer around the extracted data), and number of false positive (the lengths of unmatched extracted data).

Table 2 shows the results concerning the computation complexity and the time taken for the three methods to analyse the road centreline extraction accuracy. As can be observed from Table 2, the thinning algorithm achieved the highest computational efficiency among the three methods. The efficiency of the proposed method was intermediate, and the SCMS was the lowest.

The advantage of the proposed method was confirmed quantitatively by accuracy measures, as shown in Table 3. The results indicated that the SCMS achieved the lowest accuracy among these three methods, as it was a biased estimator for road centreline extraction. Using the proposed method, the quality values increased by up to 5.74%, 2.13%, and 1.50% compared to the results of using the thinning algorithm. The proposed method tended to obtain significantly higher accuracy than the thinning algorithm. However, the completeness of the thinning algorithm was higher than that of the proposed method because the centroids of the end regions were taken as the end points, and some lengths were lost, leading to low completeness values for the proposed method.

According to the aforementioned results, there was a trade-off between efficiency and accuracy in using the proposed method. Therefore, it can be concluded that the proposed method provides a practical solution for accurate road centreline extraction from classified images with comparatively high efficiency.

4. Conclusion

This study has proposed a method for road centreline extraction from classified images using a geodesic method. The experimental results show that the proposed method provides a more accurate extraction of road centrelines than the commonly used thinning

algorithm or the SCMS method. The implementation tested in this study used the OOF method that measures road centreline probability, but this method may be computationally expensive for processing large data sets. In further experiments, other road centreline probability estimation methods can be tested to evaluate their performances in terms of both accuracy and computational cost. This study suggests that the proposed method is a useful framework for road centreline extraction from classified images.

Funding

The work presented in this study was supported by the Ministry of Science and Technology of China [Project No.: 2012BAJ15B04, 2012AA12A305].

References

Benmansour, F., and L. D. Cohen. 2011. "Tubular Structure Segmentation Based on Minimal Path Method and Anisotropic Enhancement." *International Journal of Computer Vision* 92: 192–210. doi:10.1007/s11263-010-0331-0.

Campbell, J. B., and R. H. Wynne. 2011. *Introduction to Remote Sensing*. 5th ed. New York: The Guilford Press.

Das, S., T. T. Mirnalinee, and K. Varghese. 2011. "Use of Salient Features for the Design of a Multistage Framework to Extract Roads from High-Resolution Multispectral Satellite Images." *IEEE Transactions on Geoscience and Remote Sensing* 49: 3906–3931. doi:10.1109/TGRS.2011.2136381.

Doucette, P., P. Agouris, A. Stefanidis, and M. Musavi. 2001. "Self-organised Clustering for Road Extraction in Classified Imagery." *ISPRS Journal of Photogrammetry and Remote Sensing* 55: 347–358. doi:10.1016/S0924-2716(01)00027-2.

Genovese, C. R., M. Perone-Pacifico, I. Verdinelli, and L. Wasserman. 2013, "Nonparametric Ridge Estimation." Accessed March 1, 2014. http://arxiv.org/pdf/1212.5156v1.pdf.

Law, M. W. K., and A. C. S. Chung. 2008. "Three Dimensional Curvilinear Structure Detection Using Optimally Oriented Flux." In *Computer Vision – ECCV 2008*, edited by D. Forsyth, P. Torr, and A. Zisserman, 368–382. Berlin: Springer.

Mena, J. B. 2003. "State of the Art on Automatic Road Extraction for GIS Update: A Novel Classification." *Pattern Recognition Letters* 24: 3037–3058. doi:10.1016/S0167-8655(03)00164-8.

Miao, Z., W. Shi, H. Zhang, and X. Wang. 2013. "Road Centerline Extraction from High-Resolution Imagery Based on Shape Features and Multivariate Adaptive Regression Splines." *IEEE Geoscience and Remote Sensing Letters* 10: 583–587. doi:10.1109/LGRS.2012.2214761.

Ozertem, U., and D. Erdogmus. 2011. "Locally Defined Principal Curves and Surfaces." *Journal of Machine Learning Research* 12: 1240–1286.

Peyré, G., M. Péchaud, R. Keriven, and L. D. Cohen. 2009. "Geodesic Methods in Computer Vision and Graphics." *Foundations and Trends in Computer Graphics and Vision* 5: 197–397. doi:10.1561/0600000029.

Poullis, C., and S. You. 2010. "Delineation and Geometric Modeling of Road Networks." *ISPRS Journal of Photogrammetry and Remote Sensing* 65: 165–181. doi:10.1016/j.isprsjprs.2009.10.004.

Shi, W., Z. Miao, and J. Debayle. 2014. "An Integrated Method for Urban Main-Road Centerline Extraction from Optical Remotely Sensed Imagery." *IEEE Transactions on Geoscience and Remote Sensing* 52 (6): 3359–3372. doi:10.1109/tgrs.2013.2272593.

Shi, W., Z. Miao, Q. Wang, and H. Zhang. 2014. "Spectral–Spatial Classification and Shape Features for Urban Road Centerline Extraction." *IEEE Geoscience and Remote Sensing Letters* 11: 788–792. doi:10.1109/LGRS.2013.2279034.

Snyman, J. A. 2005. *Practical Mathematical Optimization: An Introduction to Basic Optimization Theory and Classical and New Gradient-Based Algorithms*. New York: Springer.

Soille, P. 1998. *Morphological Image Analysis: Principles and Applications*. New York: Springer-Verlag.

Spiegel, M. R., S. Lipschutz, and D. Spellman. 2009. *Vector Analysis. Schaum's Outlines*. 2nd ed. New York: McGraw Hill.

Treash, K., and K. Amaratunga. 2000. "Automatic Road Detection in Gray Scale Aerial Images." *ASCE Journal of Materials in Civil Engineering* 14: 60–69.

Wiedemann, C., C. Heipke, H. Mayer, and O. Jamet, O. 1998. "Empirical Evaluation of Automatically Extracted Road Axes." In *Empirical Evaluation Techniques in Computer Vision*, edited by K. Bowyer and P. Phillips, 172–187. Los Alamitos, CA: IEEE Computer Society.

Zhang, Q., and I. Couloigner. 2007. "Accurate Centerline Detection and Line Width Estimation of Thick Lines Using the Radon Transform." *IEEE Transactions on Image Processing* 16: 310–316. doi:10.1109/TIP.2006.887731.